



HAL
open science

Interaction between surface waves and absorbing boundaries for wave propagation in geological basins: 2D numerical simulations

G. Festa, E. Delavaud, J. -P. Vilotte

► **To cite this version:**

G. Festa, E. Delavaud, J. -P. Vilotte. Interaction between surface waves and absorbing boundaries for wave propagation in geological basins: 2D numerical simulations. *Geophysical Research Letters*, 2005, 32, pp. 639-646. 10.1029/2005GL024091 . insu-03601107

HAL Id: insu-03601107

<https://insu.hal.science/insu-03601107>

Submitted on 8 Mar 2022

HAL is a multi-disciplinary open access archive for the deposit and dissemination of scientific research documents, whether they are published or not. The documents may come from teaching and research institutions in France or abroad, or from public or private research centers.

L'archive ouverte pluridisciplinaire **HAL**, est destinée au dépôt et à la diffusion de documents scientifiques de niveau recherche, publiés ou non, émanant des établissements d'enseignement et de recherche français ou étrangers, des laboratoires publics ou privés.

Copyright

Interaction between surface waves and absorbing boundaries for wave propagation in geological basins: 2D numerical simulations

G. Festa, E. Delavaud, and J.-P. Vilotte

Département de Sismologie, Institut de Physique du Globe de Paris, Paris, France

Received 15 July 2005; revised 12 September 2005; accepted 19 September 2005; published 20 October 2005.

[1] Surface waves control the peak of the seismic records at regional and teleseismic distances. In complex structures, such as basins, their amplitude is produced by the interference between the topography and the wedges of the model. Therefore, they represent a challenging target for numerical simulations. When modelling low frequencies in thin media, such as basins and waveguides, some instabilities arise from the interaction between propagating evanescent waves and the artificial layer, required to avoid spurious reflection to be sent back into the elastic volume. Here we propose to generalize the absorbing boundary conditions, by adding a cut-off frequency and an overdamping. The efficiency is demonstrated through a comparison with analytical solutions. Finally an analysis is performed by adopting a complex basin geometry, where we show that the pollution of classical absorbing conditions becomes significant near the edges of the model. **Citation:** Festa, G., E. Delavaud, and J.-P. Vilotte (2005), Interaction between surface waves and absorbing boundaries for wave propagation in geological basins: 2D numerical simulations, *Geophys. Res. Lett.*, 32, L20306, doi:10.1029/2005GL024091.

1. Introduction

[2] Numerical methods are widely used for the simulation of wave propagation at local and regional scales. At this level the physical medium is unbounded while numerical methods are limited to a finite computational domain. Absorption on the outskirts of the model is required to mimic the unboundedness and should account for the outgoing energy to be not reflected back into the lattice. Their performance is measured through a suitable compromise between the size of the numerical mesh and the amount of spurious reflections. Exact absorbing boundary conditions force the energy to leave the lattice, but they turn out to be a non local operator in time and space on the boundary of the computational domain [e.g., *Givoli*, 1991]. It can be localized by a first-order expansion (paraxial conditions of *Clayton and Engquist* [1977]) with an efficiency at almost normal incidence. Extension to surface waves as well as to higher orders [*Higdon*, 1991] requires additional complexity. More recently, the development of Perfectly Matched Layers (PMLs) has provided an efficient absorbing condition [*Bérenger*, 1994; *Collino and Tsogka*, 2001]. PMLs have been designed to have no impedance contrast at the interface with the elastic volume and to provide an exponential decay of any propagating wave entering the layer. PMLs map the infinite space in a finite

region with the rheological characteristics of anisotropic dissipative media. They are effective for both body and surface waves but their efficiency degrades at grazing incidences, although the amplitude of the reflections remains at a reasonable low level for the most of applications. PMLs have been developed for numerical techniques, such as finite differences [*Collino and Tsogka*, 2001] and spectral elements [*Komatitsch and Tromp*, 2003; *Festa and Vilotte*, 2005].

[3] However, the bottom of the numerical grid needs to be located far from the upper edge, which is generally a free surface, to avoid that the low-frequency Rayleigh waves interfere with the absorbing layer. For such a wave, in fact, the propagation direction is parallel and not perpendicular to the edge of the PML at the bottom of the grid. In the following, we analyze the behavior of a classical PML when a surface wave penetrates into it, and we propose a generalization of the absorbing condition to avoid some instabilities. This problem is of crucial importance for the simulation of wave propagation in basins and in waveguides, where the computational volume is more stretched in the horizontal dimension than in the vertical one. The analysis is limited to 2D media, but generalization to 3D is straightforward.

2. Standard PML

[4] Consider a 2D medium, with a PML surrounding the elastic volume everywhere apart from the free surface (Figure 1). In this model, we begin by analyzing the behavior of a lateral PML, located at $0 < x < d$. In the frequency domain, a PML condition is obtained through a coordinate stretching in the complex plane [*Teixeira and Chew*, 1999]

$$\tilde{x} = x + \frac{\Sigma(x)}{i\omega} \quad (1)$$

Here ω is the frequency and Σ is an arbitrary function of x , smoothly growing from the interface to the outer boundary of the layer because of the discretization. A plane body wave

$$\Phi(x, z, t) = \mathbf{A}e^{i(\omega t - k_x x - k_z z)} \quad (2)$$

is transformed in the PML region as

$$\tilde{\Phi}(x, z, t) = \Phi(x, z, t)e^{-\frac{k_x \Sigma}{\omega}} \quad (3)$$

with an exponential decay independent of the frequency, because of the ratio k_x/ω . The same behavior applies in

the z direction. Now consider the decomposition in plane waves of a Rayleigh wave moving along the free surface $z = 0$,

$$\Psi(x, z, t) = e^{i(\omega t - k_x x)} (\mathbf{c}_\alpha e^{-\omega \tilde{\eta}_\alpha z} + \mathbf{c}_\beta e^{-\omega \tilde{\eta}_\beta z}) \quad (4)$$

Here $\tilde{\eta}_c = \sqrt{1/c_r^2 - 1/c^2}$; α , β and c_r are the P, S and Rayleigh wave speeds respectively and \mathbf{c}_α and \mathbf{c}_β are constants (for analytical expressions see, e.g., *Aki and Richards* [1980]). Since the x dependence of this wave has the same features as the body waves, it is expected to obey the same decay law (3), when entering the PML along the x direction. In addition the wave preserves the signature of a surface wave.

[5] The evanescent wave can also interact with the bottom of the model, when the vertical dimension is comparable with the largest wavelength propagated in the elastic medium. In this case, applying the transformation (1) for the z coordinate we have

$$\tilde{\Psi}(x, z, t) = e^{i(\omega t - k_x x)} (\mathbf{c}_\alpha e^{-\omega \tilde{\eta}_\alpha z} e^{i\tilde{\eta}_\alpha \Sigma} + \mathbf{c}_\beta e^{-\omega \tilde{\eta}_\beta z} e^{i\tilde{\eta}_\beta \Sigma}) \quad (5)$$

The classical decay component is enriched by a sinusoidal term $e^{i\tilde{\eta}_c \Sigma}$, which is independent of the frequency. For $\omega \rightarrow 0$, the decay term goes to zero and the Rayleigh wave is transformed into a body wave, always moving at Rayleigh wave speed. In this case, the vertical wavenumber is completely controlled by Σ , which is an increasing function of the depth [e.g., *Festa and Nielsen*, 2003]. The PML behavior for both body and surface waves is synthesized in Figure 1.

[6] For very long simulations, the instability generated in the PMLs pollutes the signal everywhere in the elastic volume. In a homogeneous medium, the coefficients \mathbf{c}_α and \mathbf{c}_β of equation (4) depend only on the wave speeds; therefore the skin-depth of the propagating wave can be estimated for any wavelength λ . At $z = \frac{\lambda}{2}$ the amplitude is reduced to the 35% of the value at the surface and at $z = \lambda$ it is at about 10%. If Λ is the largest wavelength propagated by the numerical grid, the bottom of the model should be at least located at $2-3 \Lambda$, to avoid any interference with the propagating surface wave.

3. Generalized Filtering PML (GFPML)

[7] In the frequency domain, the PML transformation (1) has a pole at $\omega = 0$. We can move it onto the imaginary axis, by changing the transformation to

$$\tilde{x} = B(x) + \frac{\Sigma(x)}{i\omega + \omega_c} \quad (6)$$

where $B(x)$ is a function of x , and ω_c is a constant. *Festa and Vilotte* [2005] have shown that, when $B(x) = x$, ω_c acts as a cut-off frequency, with an efficient absorption for $\omega > \omega_c$. On the other hand, *Kuzuoglu and Mittra* [1996] proved in electromagnetics that causality is preserved when $\frac{dB}{dx} > 1$, for any positive ω_c and $\frac{d\Sigma}{dx}$. This result can be extended to elastodynamics, almost as far as the near-field P-S coupling can be neglected. In this case, both phenomena satisfy the same wave equation.

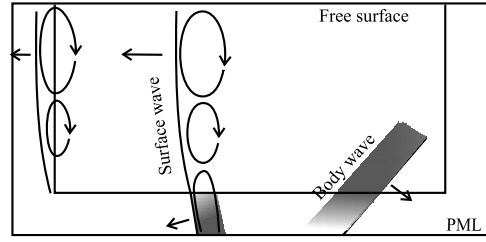


Figure 1. A simple scheme of a numerical grid for the propagation of elastic waves in the presence of a free surface and absorbing layers. A body wave is always attenuated when entering the PML. Surface waves decay exponentially when they enter the lateral PMLs, but the attenuation disappears, when they penetrate the bottom layer. Here, the evanescent waves turn into body waves and generate numerical instabilities.

[8] Adopting the transformation (6) instead of (1), the body wave decays in the PMLs as

$$\tilde{\Phi}(x, z, t) = \Phi(x, z, t) e^{ik_x \left[(B-x) - \Sigma \frac{\omega c}{\omega^2 + \omega_c^2} \right] - k_x \Sigma \frac{\omega}{\omega^2 + \omega_c^2}} \quad (7)$$

It is worth to note here that (6) is a causal Butterworth-filter transfer function, with a phase shift, that allows to preserve the causality. The exponential decay now becomes frequency dependent and it tends to classical PML as $\omega \rightarrow \infty$. The term $B(x) - x$ is a frequency-independent phase shift and it is expected to be a small contribution, growing from 0 at the PML-volume interface to some maximum value at the end of the PMLs. This layer, indeed, has almost the same behavior as the classical PML for body waves. Now we want to focus the attention on the surface waves. Again, the same transformation occurs when a surface wave enters horizontally the PML. In the case of a vertical penetration, instead, the exponentially decaying contribution $e^{-\omega \eta z}$ in (4) is transformed to

$$e^{-\omega \eta B(z) - \Sigma(z) \frac{\omega \omega_c}{\omega^2 + \omega_c^2} \eta + i \Sigma(z) \frac{\omega}{\omega^2 + \omega_c^2} \eta} \quad (8)$$

The first contribution preserves the exponential decay of a surface wave, because $B(z) \approx z$. The second one is still an exponential decay term, which goes down to zero with the order ω/ω_c . Finally the third term is a phase shift approaching zero as ω^2/ω_c^2 , steeper than the other contributions. This transformation preserves the features of a surface wave for low frequencies, without producing any artifact inside the absorbing GFPML. Before discretization, a dispersion error is produced inside the layer and it depends on the frequency. It can be evaluated and reduced, using high-order Butterworth transformations.

4. Numerical Tests

4.1. Analytical Comparison

[9] GFPML regularizes PML at the continuous level. Now we numerically test the efficiency of both methods, by comparing them to the analytical solution. We propagate a wave generated by an isotropic point source using a spectral element technique [e.g., *Festa and Vilotte*, 2005]. The model is a 2D thin homogeneous elastic medium, the

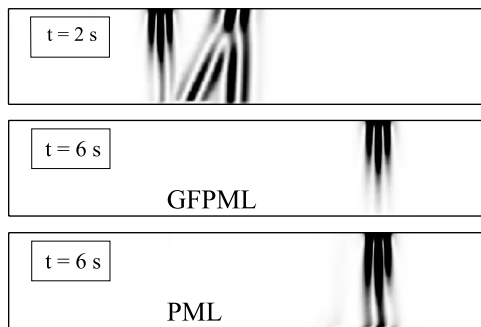


Figure 2. Snapshots of the kinetic energy at two times. The one on the top corresponds to the time $t = 2$ s, where the surface waves are separating from the body waves. Both methods give the same picture. The other two pictures are snapshots at $t = 6$ s. With GFPML, surface waves are well reproduced. When using PML, an instability is generated in the bottom layer and propagates upward.

dimensions of which are $15 \text{ km} \times 1 \text{ km}$. The elastic properties of the volume are $\rho = 2.7 \text{ g/cm}^3$, $c_p = 3.2 \text{ km/s}$ and $c_s = 1.87 \text{ km/s}$. The source is a Ricker function, with a central frequency of 2.5 Hz and a delay of 0.1 s . It is located close to the left boundary of the model, at 0.15 km from the free-surface. The medium is discretized by square elements, of size $H = 0.1 \text{ km}$, with 9 Gauss-Lobatto-Legendre collocation points and about 20 points per minimum wavelength. Finally, the time step is $4 \cdot 10^{-4} \text{ s}$.

[10] We perform two numerical experiments, in the first one the medium is surrounded by PMLs, with a Σ function growing as a quadratic power. In the second one, PMLs are replaced by GFPMLs, with the same parameters and $B(x) = x$ following a cubic law. The cut-off frequency is $f_c = 1.59 \text{ Hz}$, leading to a $\omega_c = 10 \text{ rad/s}$. In Figure 2 the snapshots of the propagation are shown at two times. The picture on the top corresponds to the time $t = 2$ s, where the surface waves are separating from the body waves. Both methods give the same result. The other two snapshots sketch the velocity field at the time $t = 6$ s. For a GFPML simulation, the surface waves are well reproduced and preserve the same features of the above snapshot (in a 2D homogeneous elastic medium surface waves do not attenuate with the distance). In the case of PMLs, the signal is generally amplified due to spurious reflections coming from the bottom. A quantitative analysis can be done by comparing the results to the analytical solution. We choose two vertical lines of receivers, located at a distance from the source of $\delta x_1 = 9 \text{ km}$ and $\delta x_2 = 11 \text{ km}$. For each line, we plot x and z components of the records for two receivers (Figure 3), one located at the surface (0.05 km beneath it) and one at 0.65 km of depth, close to the bottom of the numerical model. We can observe that for the surface records, the numerical solution provided by GFPML (dotted line) fits well the analytic curve, with an error comparable to the dispersion. The PML solution shows instead a smooth slope at the end of the signal, with an error 2 to 3 times larger than the one produced by GFPML. For the receivers located in the middle the fit is generally degraded. For GFPML, the error is at 1% for location 1 and at 4–5% for location 2. For classical PML, the amplitudes change significantly, with an error of 10% for location 1 and 18–20% for location 2, and a

low-frequency ringing at the end of the signal. When letting the simulation evolve, the instability propagates away from PML and pollutes the signal everywhere in the medium.

4.2. A 2D Geological Basin Geometry

[11] Basins have a complex structure in which amplifications are generally due to the interference between the geometrical shape (topography and wedges) and the surface waves. Here we analyze the wave propagation in a simplified model of the Caracas basin, as described by Duval *et al.* [2001]. Although we retain only the separation between sediments and bedrock, the shape preserves the geometrical complexities of basins. The rheological properties and the basin structure are shown in Figure 4a. The dimensions of the basin are about $3.0 \text{ km} \times 0.4 \text{ km}$. Waves are generated by an isotropic source, the location of which is northward, in the stiffer layer. Finally, a series of receivers has been placed on the surface. At each station, the influence of the basin has been estimated through the spectral ratio between the signal recorded with the basin and the signal obtained by

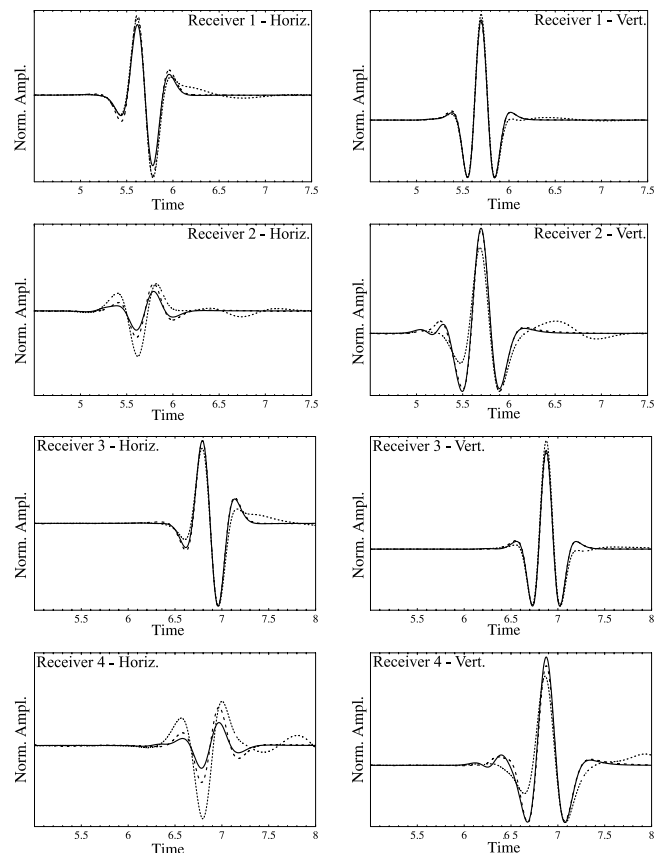


Figure 3. Horizontal and vertical component of velocity records for 4 receivers, located at $(9, 0.05)$, $(9, 0.65)$, $(11, 0.05)$, $(11, 0.65)$, all values being in km. In the pictures, the analytical solution (solid line) is compared with GFPML (dashed line) and PML (dotted line). The surface receivers measure a numerical signal consistent with the analytic one, with an error 2 to 3 times larger for PML. The error on the stations at the middle of the model is generally larger. PML attains an error of 10% and 18–20% for the second and the fourth receivers respectively against 1% to 4% for GFPML.

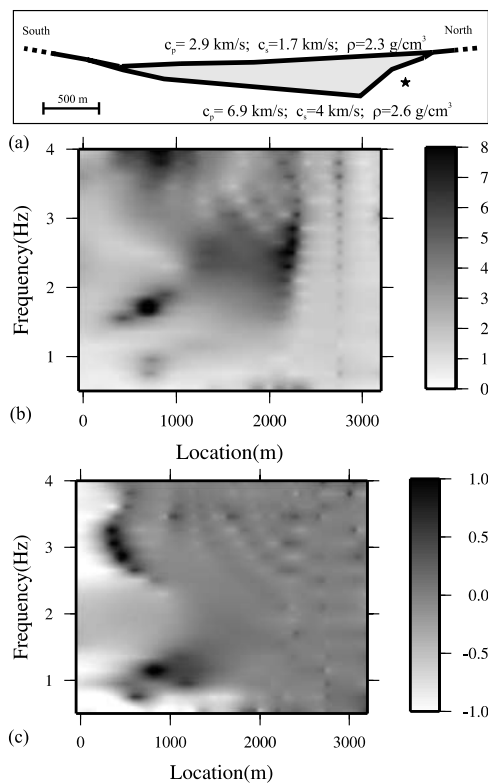


Figure 4. In the top (a), the geometrical shape of the basin with the location of the source is sketched. In the middle (b), the spectral ratio of velocity records is evaluated by using GFPML. It compares in the frequency domain, for any receiver located on the surface, the records with the basin to the records where the basin is replaced by the bedrock. The final picture (c) shows the logarithm of the ratio between the solutions with GFPML and PML, with significant differences (almost one order of magnitude) near the left wedge.

replacing the sediments with the bedrock. To account for both body and surface waves, the quadratic average of the single component spectral ratios has been plotted. In Figure 4b the solution with GFPMLs is shown. The largest amplification is at about 0.75 km with harmonics at 1.5 Hz and 3.5–4.0 Hz. In the central part of the basin the peak of amplification is around 2 Hz. In Figure 4c the logarithm of the ratio between GFPML and PML is plotted. We can see that on the left part of the basin, where surface waves are developed and interfere significantly near the wedge, the difference is almost one order of magnitude. The effect on the lower frequencies is also visible in the middle of the basin. It is necessary to double the vertical dimension to allow classical methods to superimpose to GFPML solutions.

5. Conclusions

[12] Numerical methods are widely used for the simulation of the wave propagation inside basins to model the interactions between surface waves and the topography of the sediments. We show that particular attention should be paid to the numerical mesh, which is more lengthened in horizontal direction than in the vertical one. In fact, low-frequency surface-wave trains may interact with the bottom

PML. In this case no more decay is provided inside the layer, and the surface wave loses its characteristic exponential feature. In very long simulations, this effect generates an instability, which is clearly visible everywhere in the elastic volume. When the length is about 10 times larger than the width, that is the case of several real models, the instability has no time to develop, but the effect of the absorbing boundary still pollutes the amplitude records, sometimes reaching a difference of one order of magnitude. To make the effect negligible, the bottom of the grid should be put at a double distance from the surface, significantly increasing the computation.

[13] Here we provided an analysis of this problem which identified the origin of such instabilities. When we modify PML by adding a cut-off and an overdamping (GFPML), we show that the evanescent wave features are preserved in the absorbing layer. Although a dispersion error is introduced, it goes to zero steeper than the decay term. Decay and dispersion are controlled by the filter and they can be optimized by sharpening the filter function. GFPML also provides stability in the numerical scheme, avoiding an increase of the size of the model and of the computation. Numerical tests have assessed the potential of the GFPML regularization, but a complete numerical stability analysis still remains to be done.

[14] **Acknowledgments.** We would like to thank Dimitri Komatitsch and Heiner Igel for their comments which improved the paper. We also acknowledge the Human Resources development and the mobility program of the EU, within the SPICE project, Seismic wave Propagation and Imaging in Complex Media - a European network for financial support.

References

- Aki, K., and P. Richards (1980), *Quantitative Seismology*, W. H. Freeman, New York.
- Béranger, J. (1994), A Perfectly Matched Layer for the absorption of electromagnetic waves, *J. Comput. Phys.*, *114*, 185–200.
- Clayton, R., and B. Engquist (1977), Absorbing boundary conditions for acoustic and elastic wave equations, *Bull. Seismol. Soc. Am.*, *67*, 1529–1540.
- Collino, F., and C. Tsogka (2001), Application of the PML absorbing layer model to the linear elastodynamic problem in anisotropic heterogeneous media, *Geophysics*, *66*(1), 294–307.
- Duval, A.-M., et al. (2001), Caracas, Venezuela, site effect determination with microtremors, *Pure Appl. Geophys.*, *158*, 2513–2523.
- Festa, G., and S. Nielsen (2003), PML absorbing boundaries, *Bull. Seismol. Soc. Am.*, *93*(2), 891–903.
- Festa, G., and J.-P. Vilotte (2005), The Newmark scheme as a velocity-stress time staggering: An efficient PML for spectral element simulations of elastodynamics, *Geophys. J. Int.*, *161*(3), 789–812, doi:10.1111/j.1365-246X.2005.02601.x.
- Givoli, D. (1991), Non-reflecting boundary conditions: A review, *J. Comput. Phys.*, *161*, 331–353.
- Higdon, R. L. (1991), Absorbing boundary conditions for elastic waves, *Geophysics*, *56*(2), 231–241.
- Komatitsch, D., and J. Tromp (2003), A perfectly matched layer absorbing boundary condition for the second order seismic wave equation, *Geophys. J. Int.*, *154*, 146–153.
- Kuzuoglu, M., and R. Mittra (1996), Frequency dependence of the constitutive parameters of causal perfectly matched anisotropic absorbers, *IEEE Microwave Guided Wave Lett.*, *6*, 447–449.
- Teixeira, F. L., and W. C. Chew (1999), Differential forms, metrics and the reflectionless absorption of electromagnetic waves, *J. Electromagn. Waves Appl.*, *13*(5), 665–686.

E. Delavaud, G. Festa, and J.-P. Vilotte, Département de Sismologie, Institut de Physique du Globe de Paris, F-75252 Paris Cedex 05, France. (festa@ipgp.jussieu.fr)